RSC Advances

This article can be cited before page numbers have been issued, to do this please use: M. nasrollahzadeh, M. Maham, A. rostami-vartooni, M. Bagherzadeh and S. M. Sajadi, *RSC Adv.*, 2015, DOI: 10.1039/C5RA10037B.

ROYAL SOCIETY OF CHEMISTRY

www.rsc.org/advances

View Article Online
ARTICLE TYPE www.rsc.org/xxxxxx | XXXXXXXX DOI: 10.1039/b000000x

Barberry fruit extract assisted *in situ* green synthesis of Cu nanoparticles supported on reduced graphene oxide-Fe_3O_4 nanocomposite as magnetically separable and reusable catalyst for the *O*-arylation of phenols with aryl halides under ligand-free conditions

Mahmoud Nasrollahzadeh,[a]* Mehdi Maham,[b] Akbar Rostami-Vartooni,[a] Mojtaba Bagherzadeh[c] and S. Mohammad Sajadi[d]

[a]*Department of Chemistry, Faculty of Science, University of Qom, PO Box 37185-359, Qom, Iran. E-mail: mahmoudnasr81@gmail.com; Fax: +98 25 32103595; Tel: +98 25 32850953*

[b]*Department of Chemistry, Aliabad Katoul Branch, Islamic Azad University, Aliabad Katoul, Iran*

[c]*Material Research School, NSTRI, 81465-1589, Isfahan, I. R. Iran*

[d]*Department of Petroleum Geoscience, Faculty of Science, Soran University, PO Box 624, Soran, Kurdistan Regional Government, Iraq*

Received (in XXX, XXX) Xth XXXXXXXXX 200X, Accepted Xth XXXXXXXXX 200X
First published on the web Xth XXXXXXXXX 200X
DOI: 10.1039/b000000x

In situ synthesis of copper nanoparticles (NPs) supported on reduced graphene oxide (RGO)-Fe_3O_4 nanocomposite was carried out by barberry fruit extract as a reducing and stabilizing agent. The morphology and structure of the Cu/RGO-Fe_3O_4 nanocomposite was fully characterized by means of X-ray diffraction (XRD), Fourier transformed infrared (FT-IR) spectroscopy, field emission scanning electron microscopy (FE-SEM), energy dispersive X-ray spectroscopy (EDS) and transmission electron microscopy (TEM). Cu/RGO-Fe_3O_4 was a promising catalyst for the *O*-arylation of phenols with aryl halides under ligand-free conditions. A diverse range of diaryl ethers were obtained in a good to high yield. Furthermore, due to the magnetic separability and high stability of the composite the catalyst could be separated conveniently from the reaction mixtures by an external permanent magnet and recycled multiple times without loss of catalytic activity.

Introduction

The synthesis and utilization of diaryl ethers is interesting because they are not only important structures in a variety of biologically active natural products and pharmaceuticals, but also common backbone molecules in polymer industries and materials science.[1] There are several methods for the preparation of diaryl ethers; one of the main routes is the classic Ullmann coupling reaction.[2] However, available procedures for the synthesis of diaryl ethers suffer from certain disadvantages such as harsh reaction conditions, high temperature (>200 ºC) and long reaction times, and low yields of the products, difficulty in availability or preparing the starting materials or catalysts, necessity to use stoichiometric amount of copper and expensive ligands or homogeneous catalysts, tedious work-up, waste control formation of side products, the environmental pollution caused by utilization of homogeneous catalysts.[2] These homogeneous catalysts suffer from several disadvantages as a difficult separation procedure, insufficiency in recyclability and a powerful contamination from residual metals in the reaction product.[3] To overcome these disadvantages several palladium-catalyzed coupling reactions using phosphine ligands for the synthesis of diaryl ethers have been developed.[4] However, the high cost of expensive palladium catalysts, relatively rare availability, the use of air and moisture sensitive phosphine ligands and tedious work-up in the product isolation limit their relevance for industrial applications.[5] Thus, there is a drastic need to develop a simple and practical method for the synthesis of diaryl ethers using heterogeneous copper catalyst under ligand-free conditions.

Our recent study has shown that the Cu NPs can be used as a very active catalyst for the *O*-arylation of phenols using aryl halides.[6] However, the agglomeration of Cu NPs is inevitable. An ideal support is needed to decrease NPs agglomeration.[7]

Among heterogeneous catalysts, graphene oxide (GO) and RGO have been reported as a new class of promising support and catalysts for the development of environmentally friendly acidic catalysts.[8a-c] Graphene oxide (Figure 1) can be defined as one atom thick in a closely packed honeycomb two dimensional (2D) lattice.[8] Due to its high thermal stability, good mechanical strength, high specific surface area (2630 m^2/g) and high adsorption capacity graphene has recently been garnering interest as a novel support.[8]

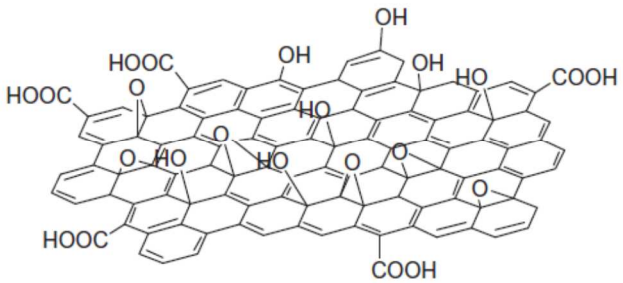

Figure 1. Proposed structure of graphene oxide (GO), reprinted with permission from ref. 8c.

Nowadays, the integration of GO (or RGO) and Fe_3O_4 into a single composite has become a hot topic of research, as it inherits the advantages of two component materials.[9] The unique properties of iron oxide-graphene based magnetic hybrid materials such as high conductivity, a large surface-to-volume ratio, strong magnetism, low cost and an environmentally benign nature have opened options for various applications.[9]

View Article Online
DOI: 10.1039/C5RA10037B

The methods which are generally adopted for the preparation of metal/RGO or metal/GO nanocomposites are chemical reduction method, physical technique and *etc*.[8] These methods are extremely expensive and also involve use of hazardous chemicals which are highly toxic and present potential environmental and biological risks. Therefore, it is desirable to develop more efficient, convenient and 'greener' methods for the synthesis of metal/RGO-Fe_3O_4 nanocomposite.

Synthesis of metal NPs using nontoxic solvents such as water, biological extracts, and environmentally benign biological methods is attractive especially if they are intended for invasive applications in medicine.[10] Greener synthesis of NPs provides advancement over physicochemical methods as it is simple, cost-effective, and relatively reproducible and often results in more stable materials.[10] Recently, we have developed the synthesis of various metal NPs using plants extract or trees gums and their catalytic activity investigation in organic synthesis.[11]

The plant of *Berberis vulgaris* from the family of *Berberidaceae*, is one of the most populated plants of Iran. Various parts of this plant including its root, bark, leaf and fruit have been used as folk medicine for a long time.[12-14] The fruit of the plant (Figure 2) is an oblong red berry 7 to 10 mm long and 3 to 5 mm broad, ripening in late summer orautumn; they are edible but very sour, and rich in vitamin C. Phytochemical analysis of different parts the plant reveals the presence of constituents such as isoquinoline alkaloids, carbohydrates, organic acids, vitamin C, polyphenolic compounds, pectin, tannin and minerals.[15] The presence of various range of phytochemicals especially vitamin C as a major antioxidant in its fruit confirmed the application of *Berberis vulgaris* fruit extract as a suitable source for simple synthesis of NPs.

Figure 2. Image of barberry fruit.

In continuation of our recent works on the green chemistry and application of heterogeneous catalysts,[7,8,11,16] we wish to report a new, green, simple, cost effective and environment friendly protocol for the preparation of Cu/RGO-Fe_3O_4 nanocomposite using barberry fruit extract as a reducing and stabilizing agent and its application as stable and heterogeneous catalyst in the *O*-arylation of phenols using aryl halides (Scheme 1). Moreover, the Cu/RGO-Fe_3O_4 nanocomposite was easily recoverable with excellent cycle stability and showed high catalytic activity for the *O*-arylation of phenols as well. To date, there is no report on the green synthesis of Cu/RGO-Fe_3O_4 nanocomposite by utilizing the fruit extract of barberry.

$$\mathrm{Ar'OH + ArX} \xrightarrow[\mathrm{Cs_2CO_3,\ DMSO,\ 120\,^{o}C,\ 12\ h}]{\mathrm{Cu/RGO\text{-}Fe_3O_4\ nanocomposite}} \mathrm{ArOAr'}$$

Scheme 1.

Results and Discussion

In this paper, we prepared a novel nanocomposite with *in situ* growth of Cu NPs attached on RGO-Fe_3O_4 as supporting material. Moreover, the catalytic activity for the *O*-arylation of phenols using aryl halides was also evaluated.

The synthetic procedure for the preparation of the Cu NPs/RGO/Fe_3O_4 nanocomposite was synthesized in four steps. The first step involves the preparation of GO from natural graphite powder by a modified Hummers method.[17] In the second step, the reduced graphene oxide (RGO) nanosheets was synthesized by the reduction of a colloidal suspension of GO based on glucose.[18] In the next step, RGO/Fe_3O_4 magnetic nanocomposite was prepared via a coprecipitation route.[19] Finally the barberry fruit extract was used for the synthesis of the Cu NPs/RGO/Fe_3O_4 nanocomposite by treating with RGO/Fe_3O_4 nanocomposite and $CuCl_2$ in water at 60 °C for 7 h.

Successful preparation of RGO from GO and fully characterized in our group recently.[18] Here, prepared RGO/Fe_3O_4 and Cu NPs/RGO/Fe_3O_4 nanocomposites are presented.

The XRD was used to examine the possible crystallinity of the RGO/Fe_3O_4 and Cu NPs/RGO/Fe_3O_4 nanocomposite. The XRD patterns of the RGO/Fe_3O_4 (a) and Cu NPs/RGO/Fe_3O_4 (b) nanocomposites are shown as Figure 3. In the 2θ range of 20-70°, the peak positions at 2θ values as 30.42, 35.57°, 42.92°, 56.62°, and 62.72° in patterns (a) and (b) are corresponded to (2 0 0), (3 1 1), (4 0 0), (5 1 1) and (4 4 0) spinel structure of Fe_3O_4, respectively.[20] It is demonstrated that Fe_3O_4 is presented in the nanocomposite and expected nanocomposites were successfully prepared. The diffraction peaks at *2θ* value of 42.92° and 53.22° corresponding, respectively, to Cu(1 1 1) and (2 0 0) crystalline plane appears, in accordance with Cu immobilization.[21]

The morphology of the RGO/Fe_3O_4 magnetic nanocomposite was determined by TEM. The average size of nanoparticles on the surface of RGO determined from Figure 4 was about 10 nm. The particles exhibited spherical morphology but with tendency to agglomeration. In general, magnetite nanoparticles synthesized through the co-precipitation are usually agglomerate. As can be seen from Figure 4, a random distribution of Fe_3O_4 nanoparticles was accrued and due to presence of Fe_3O_4 nanoparticles magnetization behaviour was expect.

View Article Online
DOI: 10.1039/C5RA10037B

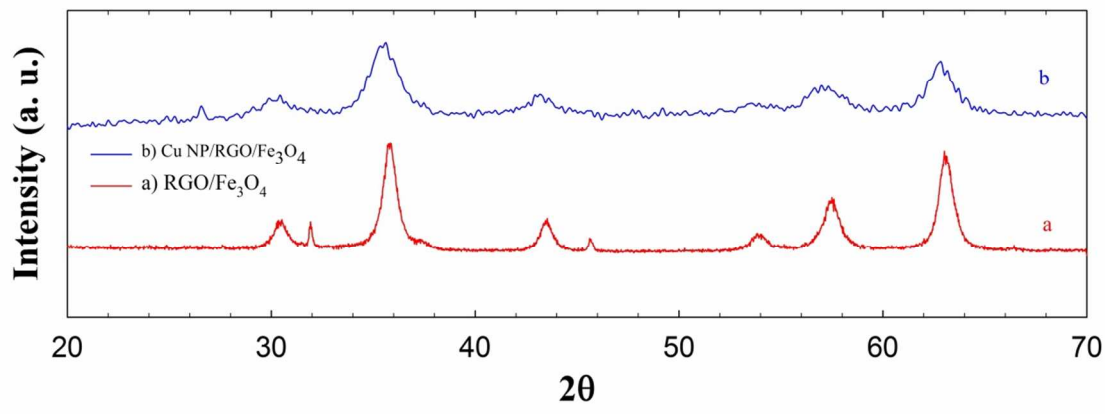

Figure 3. XRD pattern of RGO/Fe_3O_4 (a) and Cu NPs/RGO/Fe_3O_4 (b) nanocomposites.

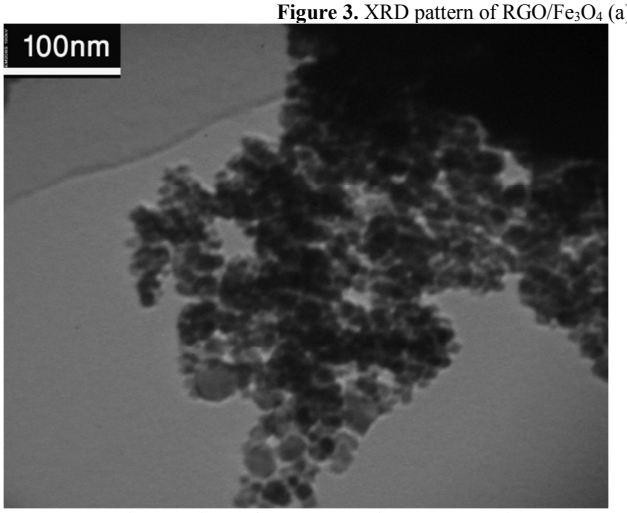

Figure 4. TEM image of RGO/Fe_3O_4 magnetic nanocomposite.

Fresh barberry fruit (*Berberis vulgaris*) was provided from Vartoon mountain area (Isfahan, Iran). The green synthesis of Cu/RGO-Fe_3O_4 nanocomposite using barberry fruit extract provides a simple, cost effective and environment friendly route without use of toxic organic solvents and hazardous and dangerous materials. Also, in this method there is no need to use high pressure, energy and temperature. Barberry fruit extract is a reducing and stabilizing agent, which favors reduction and results in the formation and distribution of Cu(0) nanoparticles on the RGO sheets without a hazardous impact on the environment.

The formation of metal nanoparticles by chemical reduction (*e.g.*, hydrazine hydrate, sodium borohydride, and ethylene glycol) may lead to absorption of harsh chemicals on the surfaces of nanoparticles raising the toxicity issue. But the present work is an environmentally friendly method (green chemistry) without use of harsh, toxic and expensive chemicals which flavonoid and phenolic acids could be adsorbed on the surface of metal nanoparticles, possibly by interaction through π-electrons interaction in the absence of other strong ligating agents.

Moreover, the UV spectrum of extract (Figure 5) shows bonds ranging λ_{max} 285 to 330 nm (bond I) due to the transition localized of π → π* related to double bonds. The extract of *Berberis vulgaris* fruits was obtained in aqueous media to extract highly polar polyhydroxyls with conjugated double bonds as major *Berberis vulgaris* constituents. Therefore, the absorption ranging 210 nm to 225 nm (bond II) is for absorbance of ring related to the benzoyl system and π → π* transitions and demonstrates the presence of phenolics. The UV spectrum of plant leaves extract show absorption bonds due to the transition localized within the conjugated system. Although, they are generally related the π → π* transitions of double bounds but this absorption bonds of cinnamoyl and benzoyl systems as shown by spectrum are finger print characteristic and specification of phenolics inside the extract as reported in literature.[22]

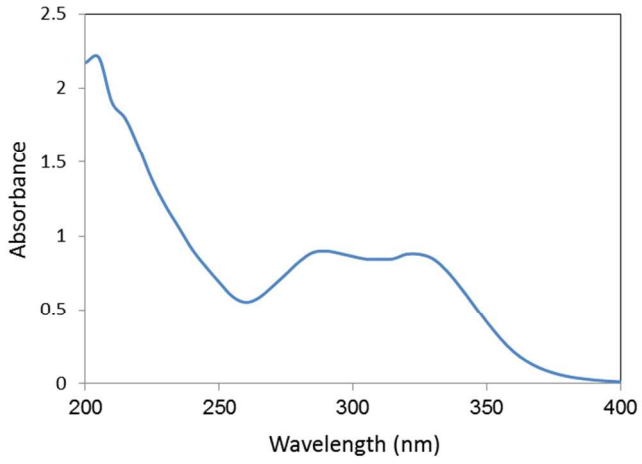

Figure 5. UV-vis spectrum of *Berberis vulgaris* fruits extract.

The UV-vis spectrum of green synthesized Cu NPs using *Berberis vulgaris* fruits extract (Figure 6) showed the significant changes in the absorbance maxima due to surface Plasmon resonance demonstrating the formation of Cu NPs. The color of the solution immediately changed into dark with λ_{max} around 550 nm indicating formation of Cu NPs as characterized by UV-vis spectrum. The synthesized Copper nanoparticles by this method are quite stable with no significant variance in the shape, position and symmetry of the absorption peak even after 20 days.

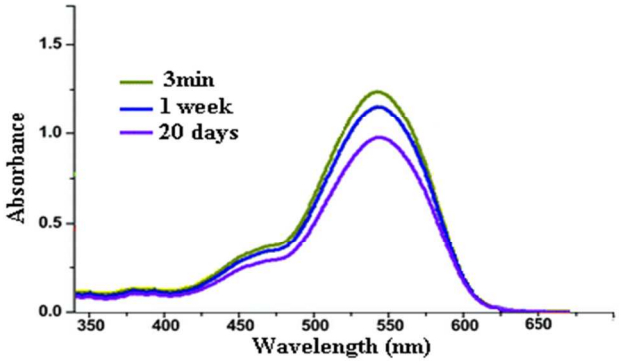

View Article Online
DOI: 10.1039/C5RA10037B

Figure 6. UV-vis spectrum of green synthesized Cu NPs using *Berberis vulgaris* fruits extract between 3 min to 20 days.

The FT-IR analysis was carried out to identify the possible biomolecules responsible for the reduction of Cu nanoparticles and capping of the bioreduced nanoparticles. The FT-IR spectrum of the crude extract (Figure 7) depicted some peaks at 3500, 1710, 1420, 1235 and 1050 cm^{-1} which represent free OH in molecule and OH group forming hydrogen bonds, carbonyl group (C=O), stretching C=C aromatic ring and C-OH and C-H stretching vibrations, respectively. These peaks suggested the presence of poly hydroxyl phenolics in the plant extract which could be responsible for the reduction of metal ions and formation of the corresponding metal nanoparticles. According to the FT-IR spectrum, flavonoid (FlOH) and phenolics acids present in the extract contributed to the reduction of copper ions and stabilization of the nanoparticles. Scheme 2 shows the probable chemical constituents present in the of barberry fruit extract responsible for the bioreduction of metal ions, their growth and stabilization. The presence of various range of phytochemicals especially vitamin C as a major antioxidant in its fruit confirmed the application of *Berberis vulgaris* fruit extract as a suitable source for simple synthesis of Cu NPs.

Furthermore, the FT-IR of Cu NPs shows demonstrative differences in the shape and location of signals indicating the interaction between $CuCl_2 \cdot 2H_2O$ and involved sites of phytochemicals for production of nanoparticles (Figure 8). Changing the location of peaks at 3400, 1720, 1432, 1300 and 1000 cm^{-1} represent the OH functional groups, carbonyl group (C=O), stretching C=C aromatic ring and C-OH stretching vibrations, respectively. Phytochemicals could be adsorbed on the surface of metal nanoparticles, possibly by interaction through π-electrons interaction in the absence of other strong ligating agents.

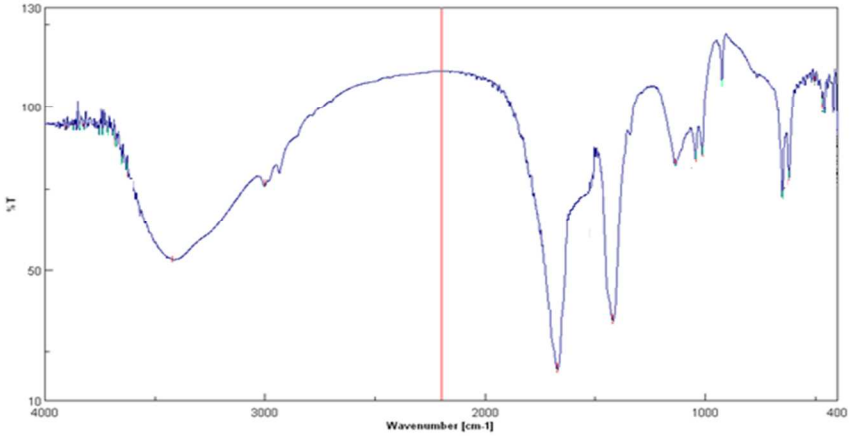

Figure 7. FT-IR spectrum of *Berberis vulgaris* fruits extract.

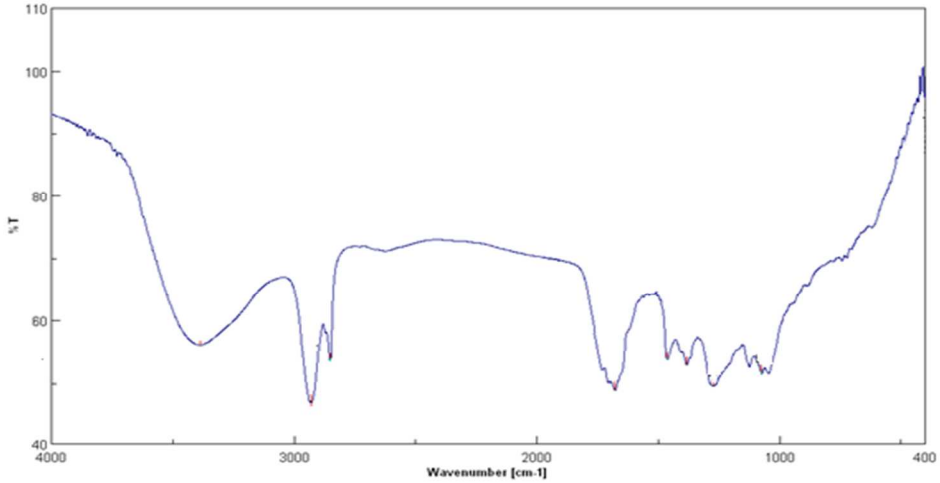

Figure 8. FT-IR spectrum of synthesized Cu NPs using *Berberis vulgaris* fruits extract.

View Article Online
DOI: 10.1039/C5RA10037B

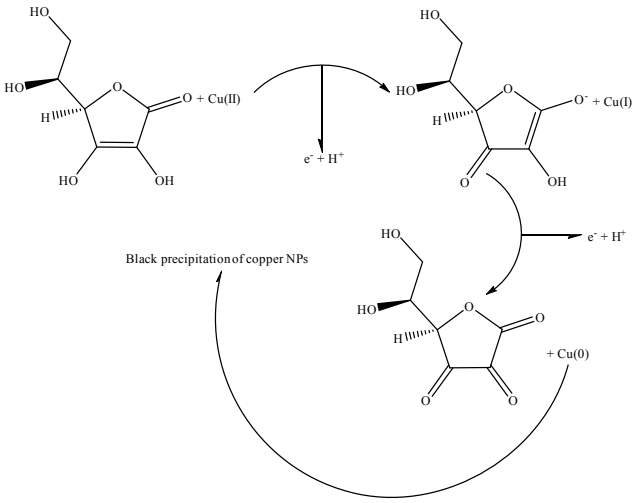

Scheme 2. Green synthesis of Cu NPs using *Berberis vulgaris* fruits extract.

XRD analysis of Cu NPs (Figure 9) show major diffraction peaks at 43.4, 50.5 and 74.5, which can be assigned to (111), (200) and (220) planes of *fcc* structure of pure Cu (JCPDS no. 85-1326). The synthesized Cu NPs were found to be pure, without any impurities like CuO, Cu_2O, $Cu(OH)_2$, etc.[6]

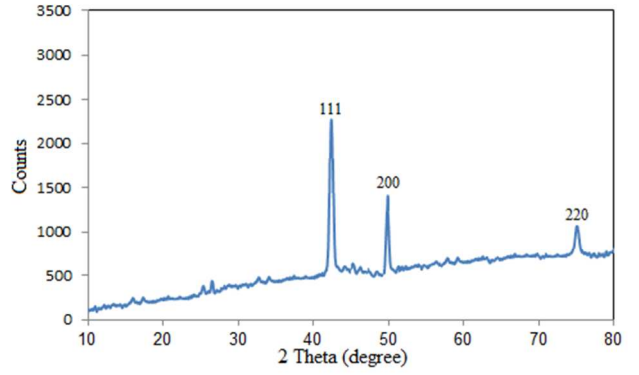

Figure 9. XRD pattern of synthesized Cu NPs using *Berberis vulgaris* fruits extract.

The FT-IR spectra of RGO/Fe_3O_4 nanocomposite and Cu NPs/RGO/Fe_3O_4 nanocomposite are shown in Figure 9. The analysis of FT-IR bands of Cu NPs/RGO/Fe_3O_4 nanocomposite shows that most of the oxygen-containing groups of GO, particularly carboxyl groups, have been removed by the reducing reaction. As expected, the FT-IR spectrum of Cu NPs/RGO/Fe_3O_4 nanocomposite is in good agreement with RGO/Fe_3O_4 (Figure 10a and 10b). An absorption band in the FT-IR spectrum of the RGO/Fe_3O_4 and Cu NPs/RGO/Fe_3O_4 nanocomposite observed at about 560 cm^{-1} which corresponds to the stretching mode of Fe-O. The broad and intense band observed in the FT-IR spectrum of the RGO/Fe_3O_4 and Cu NPs/RGO/Fe_3O_4 nanocomposite at 3403 cm^{-1} is ascribed to the stretching vibration of O-H.

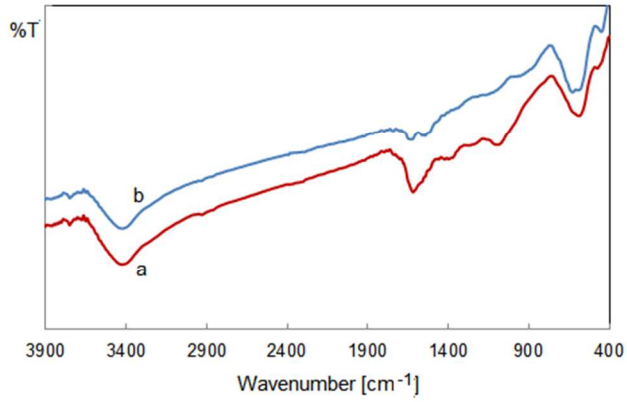

Figure 10. FT-IR spectra of (a) RGO/Fe_3O_4 nanocomposite (b) Cu NPs/RGO/Fe_3O_4 nanocomposite.

The morphology of the Cu NPs/RGO/Fe_3O_4 nanocomposite was characterized by scanning electron microscopy (SEM). Figure 11 illustrates the SEM images of the Cu NPs/RGO/Fe_3O_4 nanocomposite. The SEM image of the Cu NPs/RGO/Fe_3O_4 nanocomposite reveals that large quantities of copper nanoparticles are attached on the surface of the RGO/Fe_3O_4 nanocomposite.

To further confirm this Cu NPs/RGO/Fe_3O_4 nanocomposite structure, we take the elemental mapping by energy dispersive X-ray absorption spectroscopy (EDS). It further confirmed that the Cu NPs/RGO/Fe_3O_4 nanocomposite was composed of carbon, copper, iron and oxygen (Figure 12). The amount of Cu incorporated into the RGO/Fe_3O_4 nanocomposite found to be 11.09 w%, which determined by EDS.

The TEM image (Figure 13) of the Cu NPs/RGO/Fe_3O_4 nanocomposite shows that Cu and iron oxide nanoparticles have spherical shapes. In addition, it is observed that many copper nanoparticles with the size of about 35 nm are uniformly distributed on the RGO/Fe_3O_4 nanocomposite surfaces.

View Article Online
DOI: 10.1039/C5RA10037B

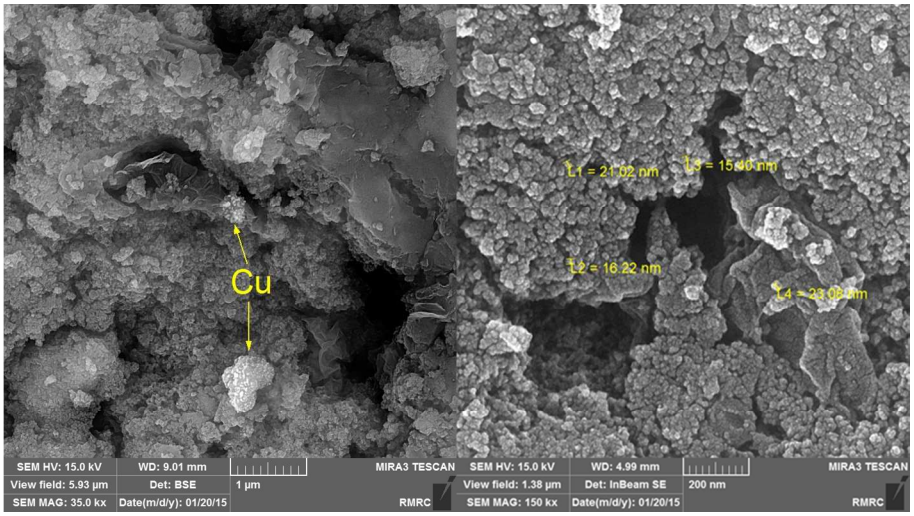

Figure 11. SEM images of Cu NPs/RGO/Fe_3O_4 nanocomposite.

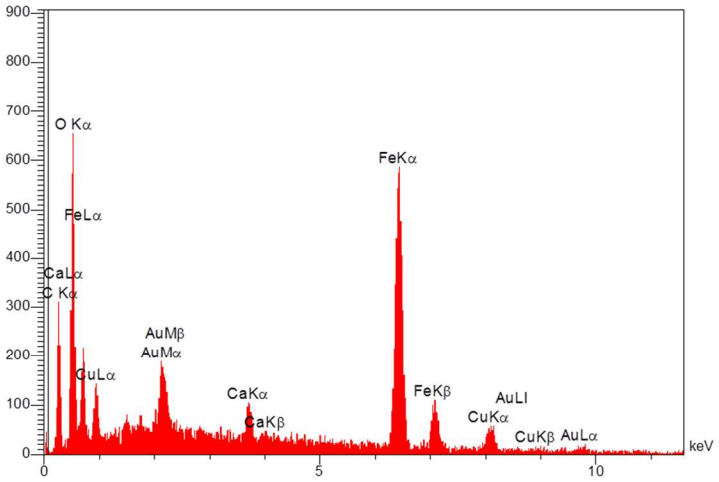

Figure 12. EDS spectrum of Cu NPs/RGO/Fe_3O_4 nanocomposite.

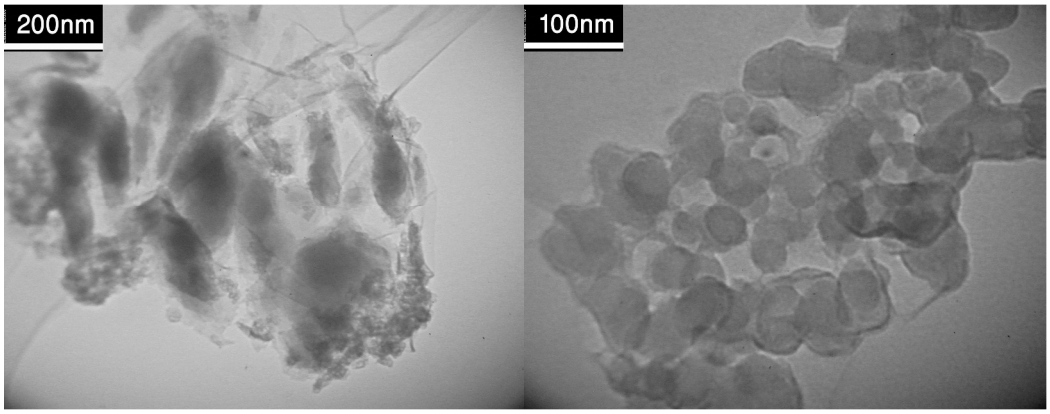

View Article Online
DOI: 10.1039/C5RA10037B

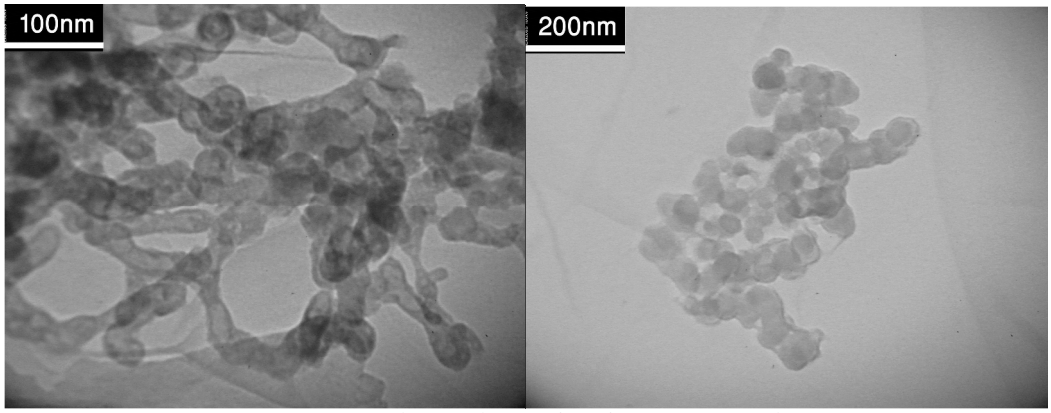

Figure 13. TEM images of Cu NPs/RGO/Fe_3O_4 nanocomposite.

In addition to that, magnetic properties of the Cu NPs/RGO/Fe_3O_4 nanocomposite were also investigated at room temperature. Figure 14 shows the hysteresis loop of Cu NPs/RGO/Fe_3O_4 nanocomposite obtained in applied magnetic field at 298 K by using a SQUID magnetometer. The magnetic saturation (Ms) value of the composite was estimated to be 22.4 emu g^{-1}. Although, the Ms values of Cu NPs/RGO/Fe_3O_4 nanocomposite was lower than that of the pure Fe_3O_4, 42 emu g^{-1},[19] but their superparamagnetic still retain the original value.

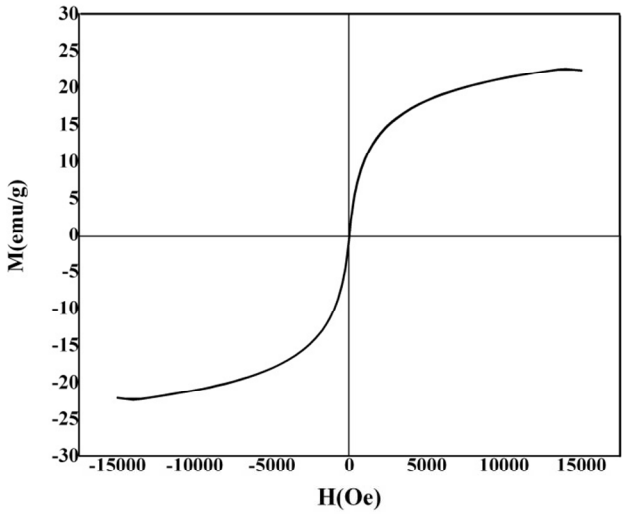

Figure 14. Room temperature magnetization curve of Cu NPs/RGO/Fe_3O_4 nanocomposites.

The Raman spectrum of Cu NPs/RGO/Fe_3O_4 nanocomposites is shown in Figure 15. The Raman spectrum of Cu NPs/RGO/Fe_3O_4 nanocomposites displays signals at 100-500 cm^{-1}, which are due to the Fe_3O_4 NPs. The peak at about 1589 cm^{-1} (G band) is corresponded to the in-phase vibration of the graphene lattice, and another peak at about 1358 cm^{-1} (D band) is related to the defects and disorder.[8d]

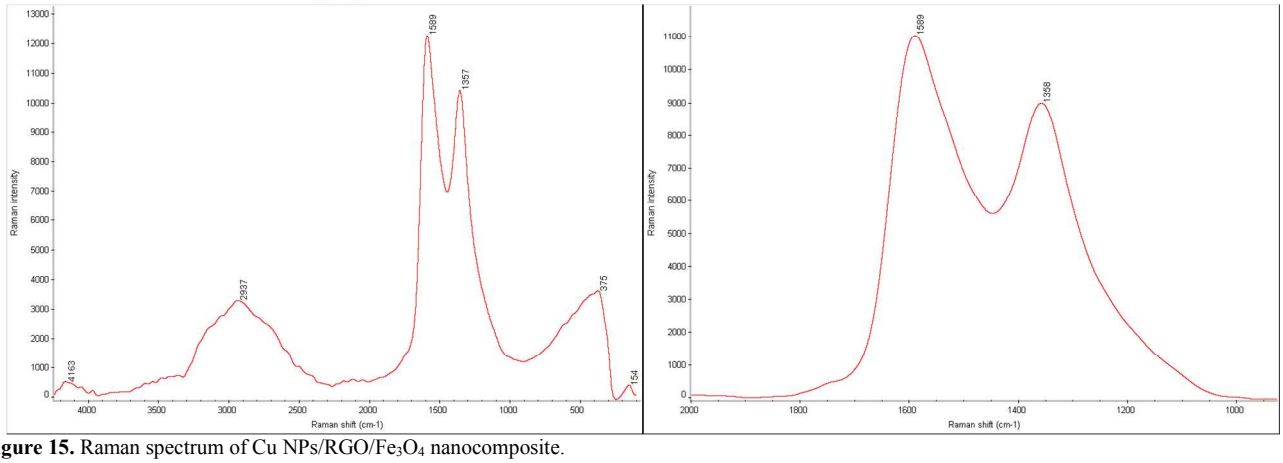

Figure 15. Raman spectrum of Cu NPs/RGO/Fe_3O_4 nanocomposite.

Evaluation of the catalytic activity of Cu NPs/RGO/Fe_3O_4 nanocomposite through the ligand-free Ullmann coupling reaction

In this work, we used Cu NPs/RGO/Fe_3O_4 as a catalyst to test the catalytic performance of this nanocomposite for the *O*-arylation of phenols using aryl halides under ligand-free conditions. In order to search for a suitable solvent, we carried out the reaction

View Article Online
DOI: 10.1039/C5RA10037B

of iodobenzene with phenol in DMSO as solvent and in the presence of Cs_2CO_3 as base and Cu NPs/RGO/Fe_3O_4 as catalyst. Some solvent including toluene, DMF and DMSO were tested in the model reaction and DMSO was selected as the best one (Table 1, entry 3). Various bases such as Cs_2CO_3, Et_3N, Na_2CO_3 and KOH were also screened for their effect on the reaction in DMSO as solvent at 120 ºC. Among the bases tested, Cs_2CO_3 was the most effective reaction base for this reaction. Also, different temperatures were also checked and 120 °C was selected as the suitable temperature. The best result was obtained with 0.05 g of Cu NPs/RGO/Fe_3O_4 nanocomposite catalyst, iodobenzene (1.0 mmol), phenol (1.0 mmol), Cs_2CO_3 (2.0 mmol) and DMSO (10.0 mL) which gave the product in an excellent yield (98%).

Table 1. Screening of base and solvents for *O*-arylation of iodobenzene with phenol.[a]

Entry	Base	Solvent	Temperature (ºC)	Yield[b] (%)
1	Cs_2CO_3	Toluene	100	10
2	Cs_2CO_3	DMF	120	72
3	Cs_2CO_3	DMSO	120	98
4	KOH	DMSO	120	36
5	Na_2CO_3	DMSO	120	62
6	Et_3N	DMSO	120	Trace
7	Cs_2CO_3	DMSO	Room temperature	12[c]
8	Cs_2CO_3	DMSO	70	52

[a]Reaction conditions: iodobenzene (1.0 mmol), phenol (1.0 mmol), base (2.0 mmol), solvent (10.0 mL), catalyst (0.05 g), 12 h, open air. [b]Isolated yield. [d]24 h

To expand the scope of this coupling reaction, various phenols and aryl halides were used as substrates under the optimized reaction conditions. The aryl halides and phenols bearing electron-donating and electron-withdrawing groups reacted well and gave good to excellent yields under the standard reaction conditions (Table 2). *Ortho*-substitution of the phenol did not hamper the cross-coupling reaction, affording products in good yield (entry 6) and no significant electronic effects were observed for *para*-substituted phenols (entries 7-10). The presence of an electron-withdrawing group on the aryl halides resulted in excellent yields for the ligand-free Ullmann coupling reactions (entries 4,5,13 and 14).

Table 2. Performance of the Cu NPs/RGO/Fe_3O_4 nanocomposite catalyst in the *O*-arylation of phenols with substituted aryl halides.[a]

$$Ar'OH + ArX \xrightarrow[Cs_2CO_3,\ DMSO,\ 120\ ^oC,\ 12\ h]{Cu/RGO\text{-}Fe_3O_4\ nanocomposite} ArOAr'$$

Entry	ArX	Ar'OH	Yield[b] (%)
1	C_6H_5I	C_6H_5OH	98
2	*p*-$CH_3C_6H_4I$	C_6H_5OH	83
3	*p*-$CH_3OC_6H_4I$	C_6H_5OH	84
4	*p*-$NO_2C_6H_4I$	C_6H_5OH	97
5	*p*-CNC_6H_4I	C_6H_5OH	97
6	C_6H_5I	*o*-$CH_3C_6H_4OH$	80
7	C_6H_5I	*p*-$CH_3OC_6H_4OH$	98
8	C_6H_5I	*p*-$CH_3C_6H_4OH$	98
9	C_6H_5I	*p*-ClC_6H_4OH	56
10	C_6H_5I	*p*-FC_6H_4OH	81
11	C_6H_5Br	C_6H_5OH	96
12	*p*-$CH_3OC_6H_4Br$	C_6H_5OH	79
13	*p*-$NO_2C_6H_4Br$	C_6H_5OH	95
14	*p*-CNC_6H_4Br	C_6H_5OH	94
15	C_6H_5Br	*p*-$CH_3C_6H_4OH$	95
16	C_6H_5Br	*p*-$CH_3OC_6H_4OH$	92
17	C_6H_5Cl	*p*-$CH_3OC_6H_4OH$	63
18	*p*-$NO_2C_6H_4Cl$	C_6H_5OH	66
19	*p*-$NO_2C_6H_4Cl$	*p*-$CH_3C_6H_4OH$	68

[a]Reaction conditions: aryl halide (1.0 mmol), phenol (1.0 mmol), Cs_2CO_3 (2.0 mmol), DMSO (10.0 mL), catalyst (0.05 g), 120 ºC, 12 h, open air. [b]Isolated yield.

We also perform a comparative study of the reactivity of Cu NPs/RGO/Fe_3O_4 nanocomposite with other reported catalysts for the synthesis of diphenyl ether via *O*-arylation of phenol with bromobenzene or iodobenzene (Table 3). With an overall look at Table 3, we can say that our method is comparable with other reported methods in term of yield and reaction time.

Compared with the other literature works on the *O*-arylation of phenol with aryl halides, the notable features of our method are:

- No requirement of inert atmosphere;
- Elimination of toxic ligands and homogeneous catalysts;
- The yield of the product is very high;
- The use of barberry fruit extract as an economic and effective alternative represents an interesting, fast and clean synthetic route for the synthesis of Cu NPs;
- Ease of handling and cost efficiency of the catalyst; and
- The catalyst can be easily recovered.

Table 3. Comparison of present methodology with other reported methods in the *O*-arylation of phenol with bromobenzene or iodobenzene for the synthesis of diphenyl ether.

Entry	Conditions (yield, %)	Ref.
1	PhBr, CuI, Meso-N-C-1, KOH, DMSO, 100 °C, 48 h (79)	23a
2	PhBr, natural clay, K_2CO_3, DMF, 110 °C, 12 h (55)	23b
3	PhI, natural clay, K_2CO_3, DMF, 110 °C, 12 h (97)	23b
4	PhBr, Cu NPs, Cs_2CO_3, DMF, 140 °C, 24 h (66)	23c
5	PhI, Cu NPs, Cs_2CO_3, DMF, 110 °C, 24 h (85)	23c
6	PhBr, silica-supported Cu(II), KF, DMSO, 130 °C, 16 h (73)	23d
7	PhI, silica-supported Cu(II), KF, DMSO, 130 °C, 16 h (92)	23d
8	PhBr, Ni-alumina, K_2CO_3, H_2O, SDS, 80 °C, 9 h (83)	23e
9	PhI, Ni-alumina, K_2CO_3, H_2O, SDS, 80 °C, 9 h (84)	23e
10	PhBr, CuI, *β*-diamide-based hybrid silica, Cs_2CO_3, MIBK, 110 °C, 22 h (87)	23f
11	PhBr, Cu-Fe-hydrotalcite, DMF, reflux, 10 h, (85)	23g
12	PhI, Cu-Fe-hydrotalcite, DMF, reflux, 7 h, (89)	23g
13	PhI, Cu_2O, ligand, Cs_2CO_3, CH_3CN, 80 °C, 24 h (93)	23h
14	PhI, CuI, TMHD, Cs_2CO_3, DMF, 60 °C, 24 h (85)	23i

View Article Online
DOI: 10.1039/C5RA10037B

15	PhI, BINAM-Cu(OTf)$_2$, Cs_2CO_3, dioxane, 110 °C, 18 h (70)	5a
16	PhBr, Cu_2O/graphene, Cs_2CO_3, THF, Ar atm., 150 °C, 3 h (26)	23j
17	PhI, Cu_2O/graphene, Cs_2CO_3, THF, Ar atm., 150 °C, 3 h (96)	23j
18	PhI, CuO NPs, Cs_2CO_3, DMSO, 110 °C, 18 h (83)	23k
19	PhI, Cu NPs, Cs_2CO_3, DMF, 120 °C, 24 h (88)	6
20	PhI, CuI, salicylaldimine ligand, K_3PO_4, dioxane, Ar atm., 101 °C, 24 h (91)	23l
21	PhBr, Cu NPs/RGO/Fe_3O_4, Cs_2CO_3, ^{t}Bu$_4$NBr, DMSO, 120 °C, 12 h (96)	This work
22	PhI, Cu NPs/RGO/Fe_3O_4, Cs_2CO_3, ^{t}Bu$_4$NBr, DMSO, 120 °C, 12 h (98)	This work

Reusability of the Cu NPs/RGO/Fe_3O_4 nanocomposite

The stability and reusability are important properties for evaluating the performance of the Cu NPs/RGO/Fe_3O_4 nanocomposite. In order to make our catalytic system greener and economical, the reusability and activity of the catalyst was also investigated for the *O*-arylation of phenol using iodobenzene. Furthermore, after the completion of the reaction the composite catalyst can be easily separated by an external magnetic field and subsequently washed with ethanol and dried and used for successive cycles. The catalyst could be reused six times without significant loss of catalytic activity (Table 4).

To check the heterogeneity of catalyst, which is an important factor, the phenomenon of leaching was studied by Inductively Coupled Plasma Atomic Emission Spectroscopy (ICP-AES) analysis of the resulting reaction solution mixture. According to the ICP analysis, very low copper contamination was observed during these experiments. These studies clearly prove that the reaction occurs heterogeneously.

Also, the nature of the recovered catalyst was investigated by EDS and SEM. EDS analysis of recovered catalyst indicates that the catalyst can be recycled six times without any significant change in the amount of Cu (Figure 16 and 17).

Table 4. Reusability of the Cu NPs/RGO/Fe_3O_4 nanocomposite in Ullmann coupling of iodobenzene with phenol.[a]

Reaction cycle	1st	2nd	3rd	4th	5th	6th
Yield[b] (%)	98%	98%	98%	96%	96%	95%

[a]Reaction conditions: iodobenzene (1.0 mmol), phenol (1.0 mmol), Cs_2CO_3 (2.0 mmol), tetrabutylammonium bromide (0.1 mmol) and DMSO (10.0 mL), catalyst (0.05 g), 120 ºC, 12 h, open air. [b]Isolated yield.

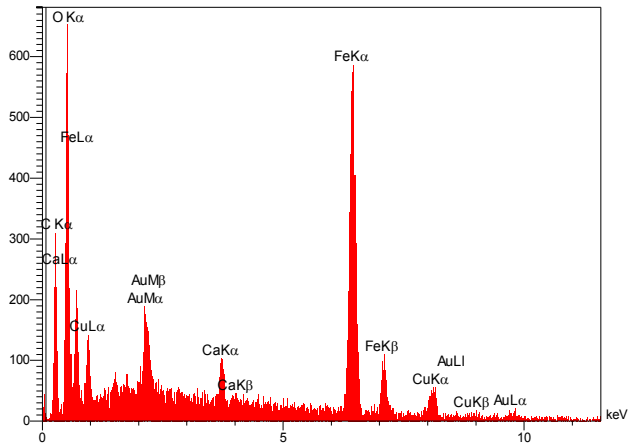

Figure 16. EDS spectrum of recovered Cu NPs/RGO/Fe_3O_4 nanocomposite.

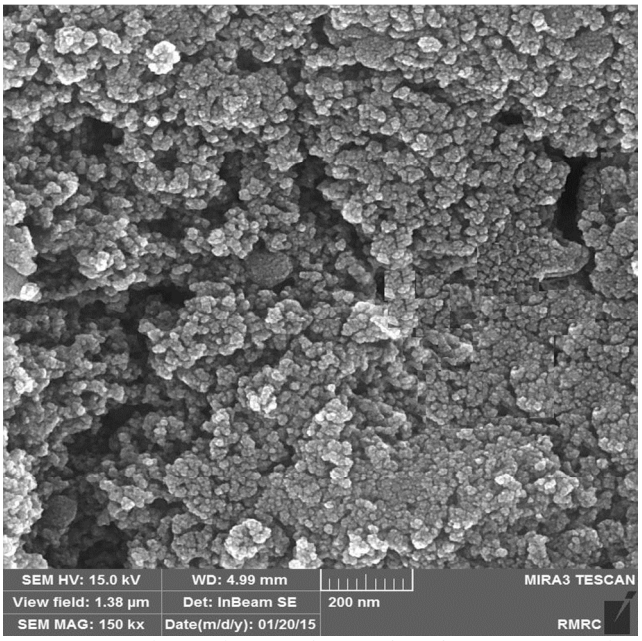

Figure 17. SEM image of recovered Cu NPs/RGO/Fe_3O_4 nanocomposite.

Conclusion

In conclusion, we have developed a novel copper-based heterogeneous magnetic catalyst by immobilizing copper NPs onto RGO/Fe_3O_4 nanocomposite via reduction of Cu^{2+} to Cu(0) by using barberry fruit extract. The use of barberry fruit extract for making metallic nanoparticles is inexpensive, easily scaled up and environmentally benign. The synthesized catalyst exhibited excellent activity for the *O*-arylation of phenols using aryl halides in a good to high yield. The catalyst could be easily recycled by means of an external magnet and reused without significant loss of catalytic activity. The simple preparation of catalyst, high efficiency of the catalyst along with high yields of products and ease of work-up under ligand-free conditions will make the present method a useful and important addition to the methodologies for the synthesis of diaryl ethers. Finally, the good catalytic properties of Cu NPs/RGO/Fe_3O_4 nanocomposite may find potential applications in various organic syntheses by taking advantage of the synergistic effects of RGO/Fe_3O_4 and Cu NPs.

Experimental

High-purity chemical reagents were purchased from the Merck and Aldrich chemical companies. All materials were of commercial reagent grade. Melting points were deter-mined in open capillaries using a BUCHI 510 melting point apparatus and are uncorrected. ^{1}H NMR and ^{13}C NMR spectra were recorded on a Bruker Avance DRX spectrometer at 300, 400 and 75, 100 MHz, respectively. FT-IR spectra were recorded on a Nicolet 370 FT/IR spectrometer (Thermo Nicolet, USA) using pressed KBr pellets. The element analyses (C, H, N) were obtained from a Carlo ERBA Model EA 1108 analyzer carried out on Perkin-Elmer 240c analyzer. The barberry fruit used in this study originated from Vartoon area, Isfahan province, Iran. X-ray

View Article Online
DOI: 10.1039/C5RA10037B

diffraction (XRD) measurements were carried out using a Philips powder diffractometer type PW 1373 goniometer (Cu Kα = 1.5406 A˚). The scanning rate was 2º/min in the 2θ range from 10 to 80˚. UV-visible spectral analysis was recorded on a double-beam spectrophotometer (Hitachi, U-2900) to ensure the formation of nanoparticles. The shape and size of Cu/RGO-Fe_3O_4 nanocomposite was identified by transmission electron microscope (TEM) using a Philips EM208 microscope operating at an accelerating voltage of 90 kV. Morphology and particle dispersion was investigated by scanning electron microscopy (SEM) (Cam scan MV2300). The chemical composition of the prepared nanostructures was measured by EDS (Energy Dispersive X-ray Spectroscopy) performed in SEM. VSM (Vibrating sample magnetometer) measurements were performed by using a SQUID magnetometer at 298 K (Quantum Design MPMS XL).

Preparation of barberry fruit extract

Fresh barberry fruit (*Berberis vulgaris*) was provided from Vartoon alpine area (Isfahan, Iran). 50 g of dried fruit powdered of *Berberis vulgaris* was added to 300 mL double distillated water in 500 mL flask and well mixed. The preparation of extract was using magnetic heating stirrer at 80 °C for 30 min. The obtained extract was filtered then filtrate was used for further experiment.

Preparation of Cu NPs using the aqueous extract of *Berberis vulgaris* fruits

In a 250 mL conical flask, 10 mL solution of $CuCl_2{\cdot}2H_2O$ 5 mM was mixed with 50 mL of the aqueous plant extract along with vigorous shaking until gradually changing the color of the mixture to dark during 3 min indicating the formation of Cu nanoparticles (as monitored by UV-vis and FT-IR spectra of the solution). The well shaked mixture then filtered and centrifuged at 7000 rpm for 30 min and obtained precipitation washed with absolute ethanol to remove possible impurities and kept under argon atmosphere.

Preparation of the RGO/Fe_3O_4 nanocomposite

The RGO/Fe_3O_4 magnetic nanocomposite with mass ratio of 1:1 was prepared via a coprecipitation route. Firstly, graphene oxide (GO) was synthesized from natural graphite powder by a modified Hummers method.[17] Then, the reduced graphene oxide (RGO) nanosheets were prepared by the reduction of a colloidal suspension of GO based on glucose.[18] Finally, the RGO/Fe_3O_4 (1:1, W/W) magnetic nanocomposite was prepared by chemical coprecipitation methods similar to our previous report for preparation of Fe_3O_4.[19] $FeCl_3.6H_2O$, $FeCl_2.4H_2O$ (2:1, mol/mol) were dissolved in HCl (25 mL, 1.0 M) solution, degassed with nitrogen gas before use. Then, the solution was added dropwise into a NaOH (250 mL, 1.5 M) solution containing prepared RGO, under vigorous stirring using nonmagnetic stirrer at 80 °C and nitrogen atmosphere. The obtained RGO/Fe_3O_4 magnetic nanocomposite was separated from the reaction medium by magnetic field, and washed with 200 mL deionized water four times, then resuspended in deionized water (100 mL).

Green synthesis of Cu/RGO-Fe_3O_4 nanocomposite using barberry fruit extract

For the synthesis of the Cu NPs/RGO/Fe_3O_4 nanocomposite, the above extract was added into prepared RGO/Fe_3O_4 nanocomposite (100 mL, 20 mg/mL) under continuous stirring. Then, 50 mL of 0.1 M $CuCl_2{\cdot}2H_2O$ was added dropwise into mixture under vigorous stirring at 60 °C for 7 h. The obtained Cu NPs/RGO/Fe_3O_4 nanocomposite was collected using an external magnetic field, washed several times with deionized water and absolute ethanol and dried in an air oven at 100 °C for 2 h. The Cu NPs/RGO/Fe_3O_4 nanocomposite catalyst was used for characterization and investigation of the catalysis.

General procedure for the ligand-free Ullmann coupling reaction

The catalyst was added to a mixture of aryl halide (1.0 mmol), phenol (1.2 mmol), Cs_2CO_3 (2.0 mmol) and DMSO (10.0 mL) and 120 °C for 12 h under open air conditions (Table 1). After completion of the reaction, mixture was cooled to room temperature, the catalyst was recovered by external magnet and washed with ethanol and dried in an oven. The resultant organic layer was extracted with ethyl acetate (25 mL). The combined organic layers were dried with anhydrous Na_2SO_4, the solvent removed and the crude product was purified by column chromatography over silica gel to provide *O*-arylated product. All the products are known compounds and the spectral data and melting points were identical to those reported in the literature.[5,6,23]

Spectral data for selected products

Diphenyl ether (Table 1, entries 1 and 11):
^{1}H NMR (300 MHz, $CDCl_3$): δ_H = 7.36-7.29 (m, 4H), 7.11-7.07 (m, 2H), 7.03-6.98 (m, 4H).

1-Methyl-4-phenoxybenzene (Table 1, entries 2, 8 and 15):
^{1}H NMR (300 MHz, $CDCl_3$): δ_H = 7.33-7.28 (m, 2H), 7.15-7.11 (m, 2H), 7.08-7.04 (m, 1H), 6.96 (d, *J* = 8.3 Hz, 2H), 6.92 (d, *J* = 8.3 Hz, 2H), 2.34 (s, 3H).

1-Methoxy-4-phenoxybenzene (Table 1, entries 3, 7, 12, 16 and 17):
^{1}H NMR (300 MHz, $CDCl_3$): δ_H = 7.33-7.27 (m, 2H), 7.05-6.87 (m, 7H), 3.79 (s, 3H).

1-Nitro-4-phenoxybenzene (Table 1, entries 4, 13 and 18):
^{1}H NMR (500 MHz, $CDCl_3$): δ_H = 8.21-8.17 (m, 2H), 7.47-7.42 (m, 2H), 7.29-7.26 (m, 1H), 7.12-7.09 (m, 2H), 7.03-7.00 (m, 2 H).

4-Phenoxybenzonitrile (Table 1, entries 5 and 14):
^{1}H NMR (500 MHz, DMSO): δ_H = 7.62-7.58 (m, 2H), 7.44-7.38 (m, 2H), 7.25-7.21 (m, 1H), 7.05 (d, *J* = 8.3 Hz, 2H), 7.01 (d, *J* = 8.3 Hz, 2H).

1-Methyl-2-phenoxybenzene (Table 1, entry 6):
^{1}H NMR (300 MHz, $CDCl_3$): δ_H = 7.33-7.25 (m, 3H), 7.20-7.15 (m, 1H), 7.08-7.00 (m, 2H), 6.93-6.90 (d, 2H), 2.25 (s, 3H).

1-Chloro-4-phenoxybenzene (Table 1, entry 9):
^{1}H NMR (400 MHz, $CDCl_3$): δ_H = 7.38-7.25 (m, 4H), 7.15-7.09 (m, 1H), 7.00-6.92 (m, 4H).

1-Fluoro-4-phenoxybenzene (Table 1, entry 10):
^{1}H NMR (400 MHz, $CDCl_3$): δ_H = 7.35-7.28 (m, 2H), 7.07 (t, *J* = 7.5 Hz, 1H), 7.05-6.94 (m, 6H).

Acknowledgement

We gratefully acknowledge the Iranian Nano Council and the University of Qom for the support of this work.

References

1 (*a*) J. Zhang, Z. Zhang, Y. Wang, X. Zheng, Z. Wang, *Eur. J. Org. Chem*., 2008, **2008**, 5112; (*b*) E. Sperotto, G. P. M. van Klink, J. G. de Vries, G. van Koten, *Tetrahedron*, 2010, **66**, 9009; (*c*) C. Sambiagio, S. P. Marsden, A. J. Blacker and P. C. McGowan, *Chem. Soc. Rev*., 2014, **43**, 3525.

2 (*a*) D. Maiti, S.L. Buchwald, *J. Org. Chem*., 2010, **75**, 1791; (*b*) F. Ullmann, *Ber. Dtsch. Chem. Ges*., 1904, **37**, 853; (*c*) E. Buck, Z. J. Song, D. Tschaen, P. G. Dormer, R. P. Volante, P. J.

View Article Online
DOI: 10.1039/C5RA10037B

Reider, *Org. Lett*., 2002, **4**, 1623; (*d*) N. Xia, M. Taillefer, *Chem. Eur. J*., 2008, **14**, 6037; (*e*) S. V. Ley, A. W. Thomas, *Angew. Chem., Int. Ed*., 2003, **42**, 5400; (*f*) G. Evano, N. Blanchard, M. Toumi, *Chem. Rev*., 2008, **108**, 3054; (*g*) Y.-J. Chen, H.-H. Chen, *Org. Lett*., 2006, **8**, 5609; (*h*) D. Ma, Q. Cai, *Org. Lett*., 2003, **5**, 3799.

3 N. R. Jogdand, B. B. Shingate, M. S. Shingare, *Tetrahedron Lett*., 2009, **50**, 4019.

4 (*a*) C. H. Burgos, T. E. Barder, X. Huang, S. L. Buchwald, *Angew. Chem. Int. Ed*., 2006, **45**, 4321; (*b*) C. A. Fleckenstain, H. Plenio, *Chem. Soc. Rev*., 2010, **39**, 694.

5 (*a*) A. B. Naidu, O. R. Raghunath, D. J. C. Prasad, G. Sekar, *Tetrahedron Lett*., 2008, **49**, 1057; (*b*) T. Miao, L. Wang, *Tetrahedron Lett*., 2007, **48**, 95.

6 M. Nasrollahzadeh, S. M. Sajadi, M. Khalaj, *RSC Adv.*, 2014, **4**, 47313

7 (*a*) M. Modarresi-Alam, M. Nasrollahzadeh, F. Khamooshi, *Sci. Iran.*, 2008, **15**, 452; (*b*) M. Modarresi-Alam, M. Nasrollahzadeh, F. Khamooshi, *Arkivoc*, 2007, **xvi**, 238; (*c*) M. Nasrollahzadeh, M. Enayati, M. Khalaj, *RSC Adv.*, 2014, **4**, 26264; (*d*) M. Nasrollahzadeh, S. M. Sajadi, A. Rostami-Vartouni, M. Khalaj, *J. Mol. Catal. A Chem*., 2015, **396**, 31; (*e*) M. Nasrollahzadeh, A. Banaei, *Tetrahedron Lett*., 2015, **56**, 500; (*f*) M. Nasrollahzadeh, S. M. Sajadi, E. Honarmand, M. Maham, *New J. Chem.*, 2015, **39**, 4745; (*g*) M. Nasrollahzadeh, S. M. Sajadi, A. Rostami-Vartooni, M. Bagherzadeh, R. Safari, *J. Mol. Catal. A Chem*., 2014, **400**, 22.

8 (*a*) P. Fakhri, B. Jaleh, M. Nasrollahzadeh, *J. Mol. Catal. A Chem*., 2014, **383-384**, 17; (*b*) M. Nasrollahzadeh, B. Jaleh, A. Jabbari, *RSC Adv*., 2014, **4**, 36713; (*c*) P. Fakhri, M. Nasrollahzadeh, B. Jaleh, *RSC Adv*., 2014, **4**, 48691; (*d*) M. Bagherzadeh, A. Farahbakhsh, "Surface functionalization of graphene", *in* "Graphene Materials: Fundamentals and Emerging Applications" A. Tiwari, M. Syvajarvi, (Edi), USA, Willy, 2015.

9 (*a*) Y. Gao, D. Ma, G. Hu, P. Zhai, X. Bao, B. Zhu, B. Zhang and D. S. Su, *Angew. Chem., Int. Ed*., 2011, **50**, 10236; (*b*) D. Yu and L. Dai, *J. Phys. Chem. Lett*., 2010, **1**, 467; (*c*) V. Chandra, J. Park, Y. J. Chun, W. Lee, I. C. Hwang and K. S. Kim, *ACS Nano*, 2010, **4**, 3979; (*d*) H. Jabeen, V. Chandra, S. J. Jung, W. Lee, K. S. Kim and S. B. Kim, *Nanoscale*, 2011, **3**, 3583; (*e*) X. Yang, X. Zhang, Y. Ma, Y. Huang, Y. Wang and Y. Chen, *J. Mater. Chem*., 2009, **19**, 2710; (*f*) Y. He, Q. Sheng, J. Zheng, M. Wang and B. Liu, *Electrochim. Acta*, 2011, **56**, 2471.

10 (*a*) E. S. Abdel-Halim, M. H. El-Rafie, S. S. Al-Deyab, *Carbohydr. Polym.*, 2011, **85**, 692; (*b*) A. R. Jasbi, *Phytochem.*, 2006, **67**, 1977; (*c*) S. P. Dubey, M. Lahtinen, M. Sillanpa, *Process Biochem*., 2010, **45**, 1065; (*d*) G. Zhan, J. Huang, M. Du, I. Abdul-Rauf, Y. Ma, Q. Li, *Mat. Lett*., 2011, **65**, 2989; (*e*) X. Huang, H. Wu, S. Pu, W. Zhang, X. Liao and B. Shi, *Green Chem*., 2011, **13**, 950.

11 (*a*) M. Nasrollahzadeh and S. M. Sajadi, *RSC Adv.*, 2015, **5**, 46240; (*b*) M. Nasrollahzadeh, M. Maham, M. M. Tohidi, *J. Mol. Catal. A Chem*., 2014, **391**, 83; (*c*) M. Nasrollahzadeh, S. M. Sajadi, M. Maham, *J. Mol. Catal. A Chem*., 2015, **396**, 297; (*d*) M. Nasrollahzadeh, S. M. Sajadi, A. Rostami-Vartooni, M. Maham, *J. Colloid. Interf. Sci*., 2015, **448**, 106.

12 C. Timothy, N. D. Birdsall, S. Gregory and N. D. Kelly, *Altern. Med. Rev.*, 1997, **2**, 94.

13 (*a*) R. Musumeci, A. Speciale, R. Costanzo, A. Annino, S. Ragusa, A. Rapisarda, M. Pappalardo, L. Iauk, *Int. J. Antimicrob. Agents*, 2003, **22**, 48; (*b*) R. Khosrokhavar, A. Ahmadiani, F. Shamsa, *J. Med. Plants*, 2010, **9**, 99.

14 (*a*) M. Fatehi, T. M. Saleh, Z. Fatehi-Hassanabad, K. Farrokhfal, M. Jafarzadeh and S. Davodi, *J. Ethnopharmacol.* 2005, **102**, 46; (*b*) M. Imanshahidi, H. Hosseinzadeh, *Phytother Res*., 2008, **22(8)**, 999.

15 (*a*) M. Sabir, *Indian J. Physiol. Pharmacol*., 1971, **15**, 111; (*b*) F. Shamsa A. Ahmadiani and R. Khosrokhavar, *J. Ethnopharmacol.*, 1999, **64**, 161.

16 (*a*) M. Nasrollahzadeh, S. M. Sajadi, M. Maham, *RSC Adv*., 2015, **5**, 40628; (*b*) M. Nasrollahzadeh, M. Maham, S. M. Sajadi, *J. Colloid. Interf. Sci*., 2015, **455**, 245.

17 N. I. Kovtyukhova, P. J. Ollivier, B. R. Martin, T. E. Mallouk, S. A. Chizhik, E. V. Buzaneva and A. D. Gorchinskiy, *Chem. Mater.*, 1999, **11**, 771.

18 M. Bagherzadeh, M. Heydari, *Analyst*, 2013, **138**, 6044 and references therein.

19 M. Bagherzadeh, M. Pirmoradian, F. Riahi, *Electrochimica Acta*, 2014, **115**, 573.

20 M. Bagherzadeh, S. Ansari, F. Riahi, A. Farahbakhsh, *Int. J. Electrochem*., 2013, Article ID 803672.

21 N. Hussain, P. Gogoi, V. K. Azhaganand, M. V. Shelke and M. R. Das, *Catal. Sci. Technol*., 2015, **5**, 1251.

22 S. V. Bhat, B. A. Nagasampagi, M. Sivakumar, *Chemistry of natural products*, Narosa publishing house, new delhi, 2005, p. 585.

23 (*a*) P. Zhang, J. Yuan, H. Li, X. Liu, X. Xu, M. Antonietti and Y. Wang, *RSC Adv.*, 2013, **3**, 1890; (*b*) R. Arundhathi, B. Sreedhar, G. Parthasarathy, *Appl. Clay. Sci*., 2011, **51**, 131; (*c*) Yuto Isomura, Takashi Narushima, Hideya Kawasaki, Tetsu Yonezawa and Yasushi Obora, *Chem. Commun*., 2012, **48**, 3784; (*d*) Tao Miao and Lei Wang, *Tetrahedron Lett*., 2007, **48**, 95; (*e*) A. Ghatak, S. Khan, R. Roy, S. Bhar, *Tetrahedron Lett*., 2007, **48**, 95; (*f*) S. Benyahya, F. Monnier, M. W. Chi Man, C. Bied, F. Ouazzani and M. Taillefer, *Green Chem.*, 2009, **11**, 1121; (*g*) V. R. Choudhary, D. K. Dumbre, P. N. Yadav, S. K. Bhargava, *Catal. Commun*., 2012, **29**, 132; (*h*) A.-Y. Cheng, J.-C. Hsieh, *Tetrahedron Lett*., 2012, **53**, 71; (*i*) F.-F. Yong, Y.-C. Teo, Y.-K. Yan, G.-L. Chua, *Synlett*, 2012, **23**, 101; (*j*) Z. Zhai, X. Guo, Z. Jiao, G. Jin and X.-Y. Guo, *Catal. Sci. Technol*., 2014, **4**, 4196; (*k*) J. Zhang, Z. Zhang, Y. Wang, X. Zheng, Z. Wang, *Eur. J. Org. Chem*., 2008, 5112; (*l*) C.-W. Qian, W.-L. Lv, Q.-S. Zong, M.-Y. Wang, D. Fang, *Chin. Chem. Lett*., 2014, **25**, 337; (*m*) P. Mondal, A. Sinha, N. Salam, A. Singha Roy, N. R. Jana and S. M. Islam, *RSC Adv.*, 2013, **3**, 5615.